ELSEVIER

Polymer 43 (2002) 1453–1460

polymer

www.elsevier.com/locate/polymer

The polydispersity of ethylene sequence in metallocene ethylene/α-olefin copolymers III: crystallization and melting behavior of short ethylene sequence

Fajun Zhang[a], Mo Song[b], Tongjian Lü[c], Jieping Liu[a], Tianbai He[a,*]

[a]*State Key Laboratory of Polymer Physics and Chemistry, Changchun Institute of Applied Chemistry, Chinese Academy of Sciences, Changchun, Jilin 130022, People's Republic of China*

[b]*IPTME, Loughborough University, Loughborough LE11, 3TU, UK*

[c]*College of Chemical Science and Engineering, Liaoning University, Liaoning 110036, People's Republic of China*

Received 23 April 2001; received in revised form 24 July 2001; accepted 27 August 2001

Abstract

Crystallization and melting behavior of short ethylene sequence of metallocene ethylene/α-olefin copolymer with high comonomer content have been studied by standard DSC and modulated-temperature differential scanning calorimetry (M-TDSC) technique. In addition to high temperature endotherm around 120°C, a low temperature endotherm is observed at lower temperatures (40–80°C), depending on time and temperature of isothermal crystallization. The peak position of the low temperature endotherm T_m^{low} varies linearly with the logarithm of crystallization time and the slope, D, decreases with increasing crystallization temperature T_c. The T_m^{low} also depends on the thermal history before the crystallization at T_c, and an extrapolation of T_m^{low} (30.6°C) to a few seconds has been obtained after two step isothermal crystallization before the crystallization at 30°C. The T_m^{low} is nearly equal to T_c, and it indicates that the initial crystallization at low temperature is nearly reversible. Direct evidence of conformational entropy change of secondary crystallization has been obtained by using M-TDSC technique. Both the M-TDSC result and the activation energy analysis of temperature dependence suggest that crystal perfection process and conformational entropy decreasing in residual amorphous co-exist during secondary crystallization.

Keywords: Metallocene ethylene/α-olefin copolymer; Modulated-temperature differential scanning calorimetry; Polydispersity

1. Introduction

This paper is the third in a series dealing with the polydispersity of ethylene sequence length in ethylene/α-olefin copolymers. In the preceding papers [1,2], the concept of polydispersity has been introduced to describe the heterogeneity of ethylene sequence. Polydispersity is a typical feature of soft matter and it presents the fluctuation of their particles on size. The polydispersity of polymers usually embodies as the heterogeneous of molecular weight and the polydispersity of sequence length is special for copolymers. The random distribution of non-crystallizable co-unit in ethylene/α-olefin copolymers leads to the polydispersity of ethylene sequence length in this system. Three basic features should be considered when studies are carried out: (1) the ethylene sequences are crystalline chain segements; (2) the sequence length is usually in micro or nanoscale dimension; (3) the intra-molecular sequences are connected by covalent bond. In our previous paper [1], the influences of polydispersity of ethylene sequence length on crystallization and melting behavior have been studied. It is concluded that intensive properties (such as crystallization and melting temperatures) are controlled not by the average sequence length but by the fluctuation of ethylene sequences on size; the extensive properties (crystallization enthalpy and crystallinity) decrease with decreasing average sequence length. Further studies by using thermal fractionation technique [2] on the polydispersity of ethylene sequence length and the nanoscale crystal phases show that the nanoscale crystal phases formed by ethylene sequence with different length really exist in these systems and both the sequence length and the crystal size broadness indexes are obtained. The broadness indexes of solvent gradient fractionation (SGF) fractions are larger than that of cross-fractionation (CF) fractions. For a given fraction, lamellar thickness distribution is more uniform than that of

* Corresponding author. Tel.: +86-431-526-2123; fax: +86-431-526-2126.

E-mail address: tbhe@ns.ciac.jl.cn (T. He).

0032-3861/02/$ - see front matter
PII: S0032-3861(01)00670-X

sequence length. The broadness index changes a little with molecular weight and the average sequence length decreasing with increasing molecular weight whereas average lamellar thickness increases with molecular weight.

In this report, crystallization and melting behavior of short ethylene sequence was studied by considering the third feature of the polydispersity of ethylene sequence mentioned above i.e. the intra-molecular sequences are connected by covalent bond. Flory's equilibrium model [3] states that at a given temperature, only the fraction of ethylene sequences of length greater than critical length can participate in the crystallization process. Thus, in ethylene/α-olefin copolymer system, the long sequences should first crystallize at the highest temperature, and on further cooling shorter ethylene sequence begins participating in the crystallization process. So the crystallization of short ethylene sequence is in a constrained environment [4].

The crystallization and melting behavior of ethylene/α-olefin copolymers have been widely studied [4–18]. However, only a few works [4] focus on the secondary crystallization of short ethylene sequences in a constrained environment. Alizadeh et al. studied the influence of structural and topological constraints on the crystallization and melting behavior of ethylene/1-octene copolymers [4]. Their results indicated that the crystallization mechanism of short ethylene sequence is quite different from that of the long sequences, and the upward shift of the melting endotherm of secondary crystals with longer crystallization time is explained by a decrease in the molar conformational entropy of the remaining amorphous fraction as a result of secondary crystallization. Generally, the time and temperature dependence of low temperature endotherm for semicrystalline polymers can be envisaged as a slow transformation to which, in principle, several phenomena can contribute [19]: lamellar thickening, reorganization of amorphous regions, rejection of defects from crystals, and crystallization of amorphous chain segments. Up to now, there is no direct evidence supporting the molar conformational entropy change of the remaining amorphous fraction during secondary crystallization.

In recent years, the modulated-temperature differential scanning calorimetry (M-TDSC) technique is growing in popularity since its introduction a few years ago [20]. One of the physical quantity obtained from M-TDSC is the imaginary part of complex heat capacity, C''_p. Schawe [21] and Hutchinson et al. [22] discussed the physical meaning of C''_p, and Schawe [21] indicated that C''_p is connected with the time-dependent processes which includes information about the internal entropy change. Song [23,24] studied the physical aging of polymer by M-TDSC, and derived the relationship of ΔS and C''_p. The results show that with increasing annealing time, the peak of the imaginary part of the complex heat capacity becomes narrow, but the peak area changes a little, which indicated that C''_p is not correlated with relaxation enthalpy but with entropy.

In this paper, crystallization and melting behavior of short ethylene sequences were investigated by standard DSC and M-TDSC, and the direct evidence of internal entropy change during secondary crystallization is shown.

2. Experimental

2.1. Materials

The polymer materials examined in this study were narrow molecular weight distribution (MWD) metallocene catalyzed short-chain branched polyethylene fractions obtained by using SGF and CF techniques [25]. Detailed molecular characteristics of these fractions have been shown in our proceeding paper [1,2]. In this work, one of SGF fraction (SGF4 comonomer content 8.04% mole percent, $M_w = 19700$ and $M_w/M_n = 1.13$) was used to study the crystallization and melting behavior of short ethylene sequences.

2.2. Instrument and measurements

DSC experiments were conducted on a computerized Perkin–Elmer differential scanning calorimeter, Model DSC-7. The specimens were weighed in the range 3–5 mg. The temperature reading and calorific measurement were calibrated by using standard indium.

M-TDSC: A TA Instruments 2920 M-TDSC calorimeter was used. Oscillation amplitude of ±0.2°C and an oscillation period of 60 s with a heating rate of 2°C/min were used. The calorimeter was calibrated with a standard indium sample. From 2920 M-TDSC, the following important signals can be obtained directly.

1. Heat flow
2. Complex heat capacity, C^*_p
3. Reversing heat flow (or reversing heat capacity, C'_p)
4. Non-reversing heat flow (or non-reversing heat capacity, C^n_p)
5. Phase angle, ϕ ($\tan\phi = C''_p/C'_p$)
6. Dynamic heat capacity C''_p (imaginary part)

$$C^*_p = C'_p + iC''_p$$

3. Results

3.1. Time and temperature dependence of crystallization and melting behavior of short ethylene sequences

Fig. 1 shows the cooling and subsequent heating curves of SGF4, the rate is 10°C/min. As observed in previous studies, the crystallization process of ethylene/α-olefin copolymers takes place over a very wide temperature range. Upon cooling from the melt, the crystallization process is characterized by a sharp high temperature exotherm, followed immediately by a broader exotherm extending to much lower temperature. The heating curve is characterized by

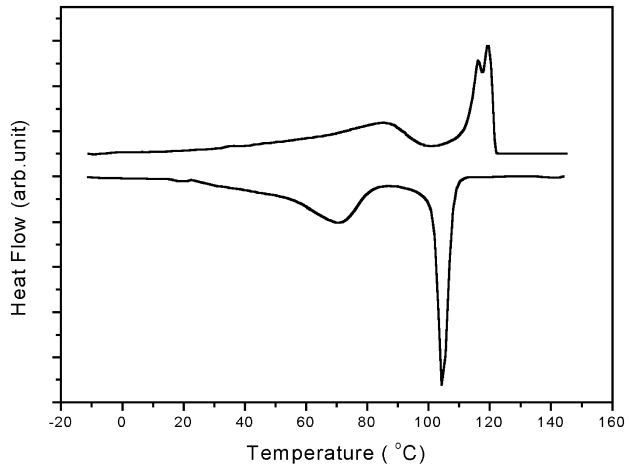

Fig. 1. DSC cooling and subsequent heating curves of SGF4 fraction, scanning rate 10°C/min.

three melting peaks. It is obvious that the broad low temperature endotherm corresponds to the broad exotherm in the cooling scan. The double-peak melting behavior of high temperature is similar to that of isothermal crystallization lower than 114°C as reported in our previous work [1], in which the highest melting endotherm has been demonstrated as the melting of crystals formed by recrystallization process. In this work, just the low temperature broad exotherm and endotherm are mainly discussed.

Fig. 2 shows the time dependence of low temperature endotherm after isothermal crystallization at 30°C for various times. The sample was quenched from 160 to 30°C and held at this temperature for different periods of time. After further crystallization at 30°C the samples were further quenched to −20°C and immediately reheated at a rate of 10°C/min. The melting curves of sample crystallized at 30°C for various times reveal the presence of a low temperature endotherm even for the shortest time. The low temperature endotherm increases in magnitude and shifts toward higher temperatures for longer crystallization times. In contrast, the location of higher melting endotherms does not affect by the crystallization process.

Fig. 3 shows the influence of temperature on secondary crystallization. The heating curves of 30 min for different temperatures are selected. The series of crystallization process are very similar to that of crystallization at 30°C as indicated in Fig. 2. The samples were also quenched from the melt to the desired crystallization temperature T_c, and maintained at that temperature for a given time, t_c. Then the samples were further quenched to −20°C, and immediately reheated at a rate of 10°C/min. For all temperatures from 25 to 70°C, the presence of a low temperature endotherm is detected for crystallization times as short as 1 min. This phenomenon indicates that the induction time is not required to detect the endothermic peak.

The dependence of the low temperature endotherm T_m^{low} on log t_c can be expressed by [4]:

$$T_m^{low} = T_0 + D \log(t_c) \quad (1)$$

where T_0 is the melting temperature of crystals at the beginning of the secondary crystallization, and D is a temperature dependent parameter. The plots of T_m^{low} vs. $\log(t_c)$ for crystallization between 30 and 60°C for SGF4 are shown in Fig. 4. We see that in all cases T_m^{low} varies linearly with the logarithm of time. However, the plots are not parallel to each other, the slopes D decrease with increasing secondary crystallization temperature T_c (see Table 1). The intersections are all several degrees higher than T_c. In Section 3.2, we will show that the intersections (extrapolation of T_m^{low} to a few seconds) are strongly affected by thermal history. In the work by Alizadeh et al. [4], when T_c is lower than 50°C, T_m^{low} vs. log t_c plots are parallel and extrapolation of T_m^{low} to times of a few seconds consistently yielded T_c, which is different from our results.

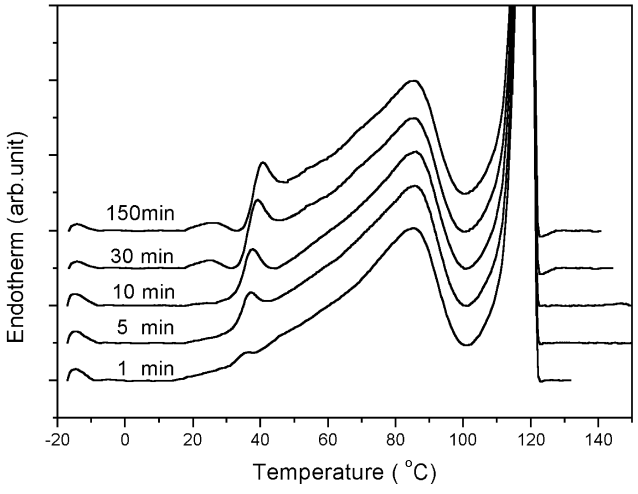

Fig. 2. Evolution of the melting behavior for SGF4 after quenching from 160 to 30°C, crystallization at 30°C for various times from 1 to 150 min, and subsequent quenching to −20°C.

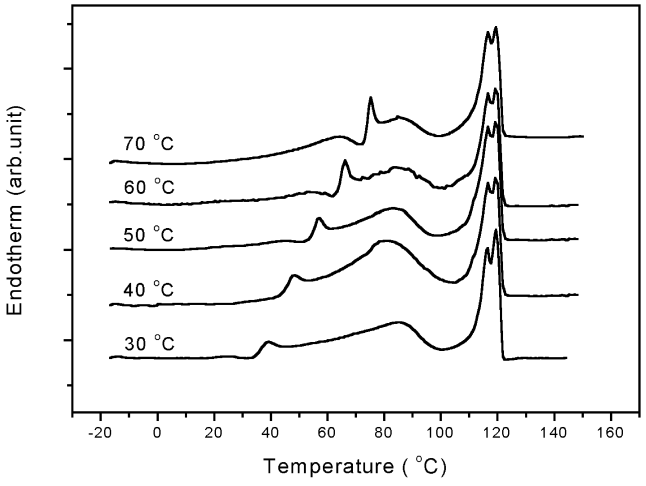

Fig. 3. Heating curves for SGF4 crystallized for 30 min at temperatures between 30 and 70°C and subsequently quenched to −20°C.

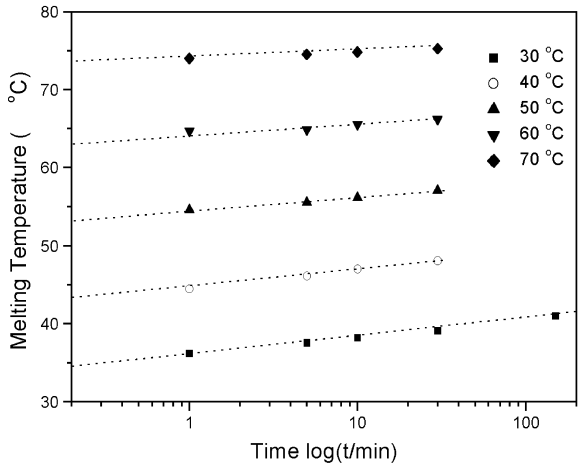

Fig. 4. Plots of T_m^{low} vs. log t for crystallization between 30 and 60°C.

3.2. Effect of thermal history on the time dependence of low temperature endotherm

As described in Section 3.1, the secondary crystallization was carried out after the crystallization of long sequence, thus the environment of secondary crystallization strongly depends on the primary crystallization of long sequence. Fig. 5a shows three different roads for secondary crystallization at 30°C. In road A, the sample was quenched from melt directly to the secondary crystallization temperature, which is similar to the process described earlier. In road B, the sample was crystallized at 110°C for 30 min before quenching to 30°C. In road C, the sample was crystallized at 110 and 70°C for 30 min, respectively before quenching to 30°C. Our previous work [1] indicates that the time of 30 min is enough to complete the crystallization of long sequence at 110°C. In road A, the long sequences crystallized almost at 105°C as indicated in Fig. 1, and the quenching process lead to more defects in system. Whereas isothermal crystallization at 110 and 70°C for 30 min should perfect the crystals. Fig. 5b shows the time dependence of secondary crystallization for different road. We see that the linearships are parallel to each other but shift vertically. The extrapolation of T_m^{low} for road C to times of a few seconds gives T_m^{low} (30.6°C) which is just slightly higher than 30°C. This result indicates that the stepwise crystallization can decrease melting temperature of the secondary crystallization. The fact that the T_m of crystals at the beginning of the secondary crystallization for road C is almost equal to the crystallization temperature indicates that the secondary crystallization need no supercooling and crystallization

Table 1
Parameters of Eq. (1) obtained from Fig. 4

T_c (°C)	25	30	40	50	60	70
T_0 (°C)	30.9	36.1	44.5	54.5	64.5	74.0
D	2.41	2.18	2.08	1.67	1.06	0.86

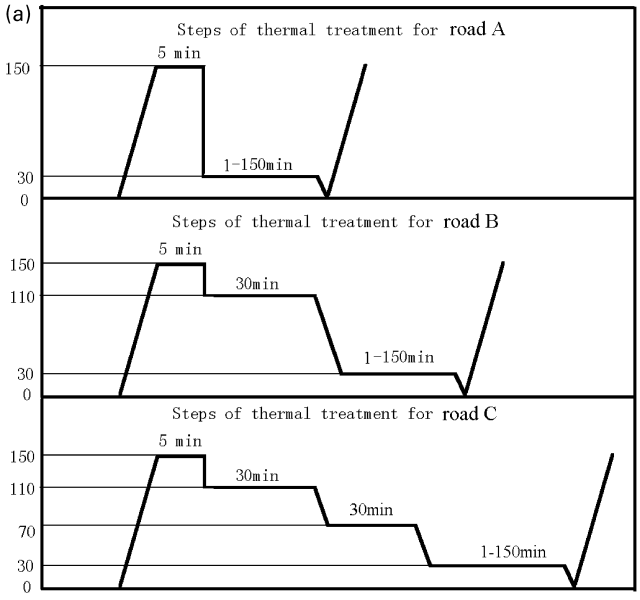

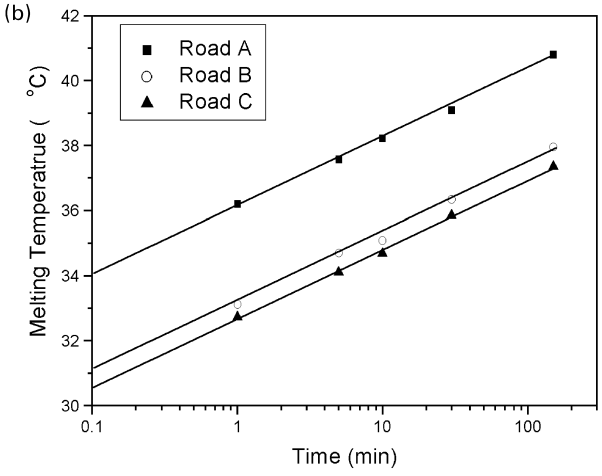

Fig. 5. (a) Schematic drawing of three roads of secondary crystallization at 30°C. (b) Plots of T_m^{low} vs. log t for crystallization at 30°C via different roads as indicated in Fig. 5a.

and melting behavior are almost reversible. The slopes of plots of T_m^{low} vs. log t_c change little indicating that the long time crystallization at low temperature does not affect the linearship between T_m^{low} and log t_c but the relative values of T_m^{low}. The perfection of crystal formed during quenching form melt to 30°C also contributes to the low temperature endotherm, but in the same magnitude for different crystallization time and this effect can be reduced by stepwise crystallization process.

3.3. Entropy change during secondary crystallization directly detected by M-TDSC

In order to obtain a measure of the 'conformational entropy change' for secondary crystallization, secondary crystallization experiments were conducted on M-TDSC.

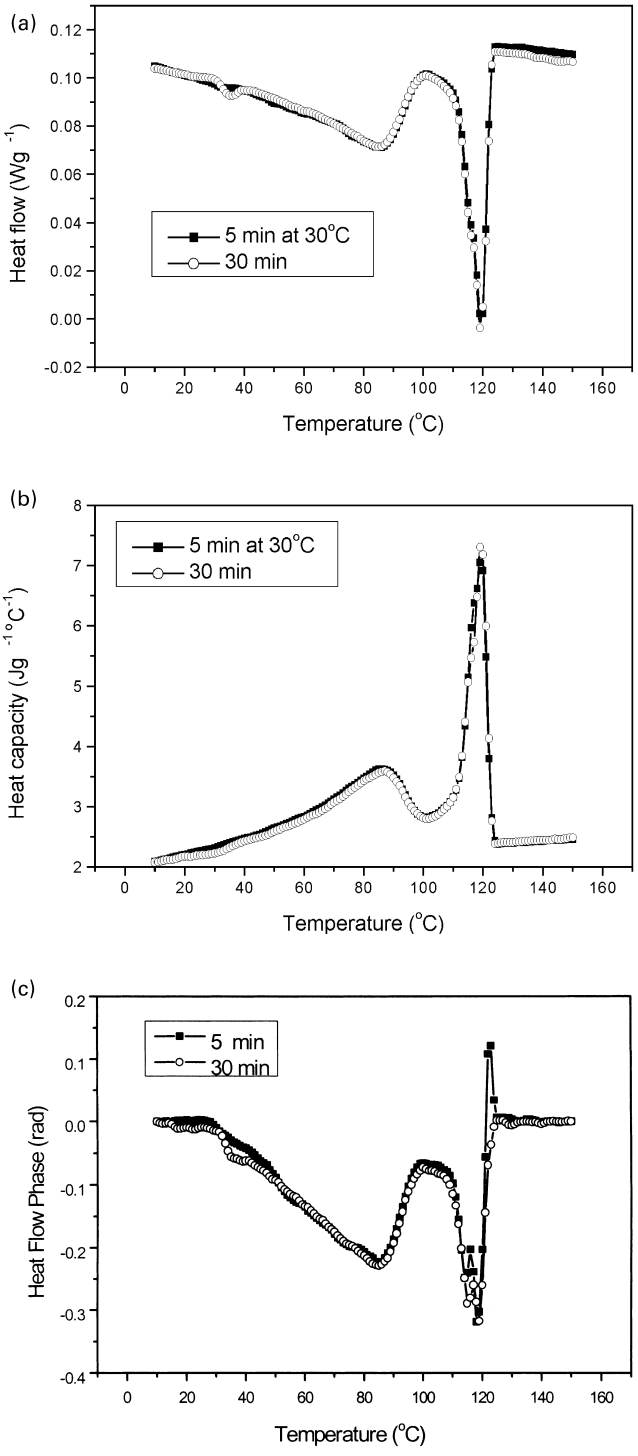

Fig. 6. Plots of (a) heat flow, (b) complex heat capacity and (c) heat flow phase angle as a function of temperature obtained directly from M-TDSC after crystallization at 30°C for 5 and 30 min.

Fig. 6 shows the plots of heat flow (a), complex heat capacity C''_p (b) and heat flow phase angle ϕ (c) as a function of temperature for secondary crystallization at 50°C for 5 and 30 min. All these signals are obtained directly from M-TDSC except heat flow phase angle which was subtracted before plotting. The imaginary part of complex heat capacity C''_p can be easily obtained by using $C''_p = C^*_p \sin \phi$. One can see from Fig. 6 that although heat flow changes obviously with increasing time of secondary crystallization, the complex heat capacity changes little with time. Fig. 7a shows the plots of C''_p as a function of temperature for secondary crystallization at 30°C for 5 and 30 min. Fig. 7b and c shows the local plots of Figs. 6a and

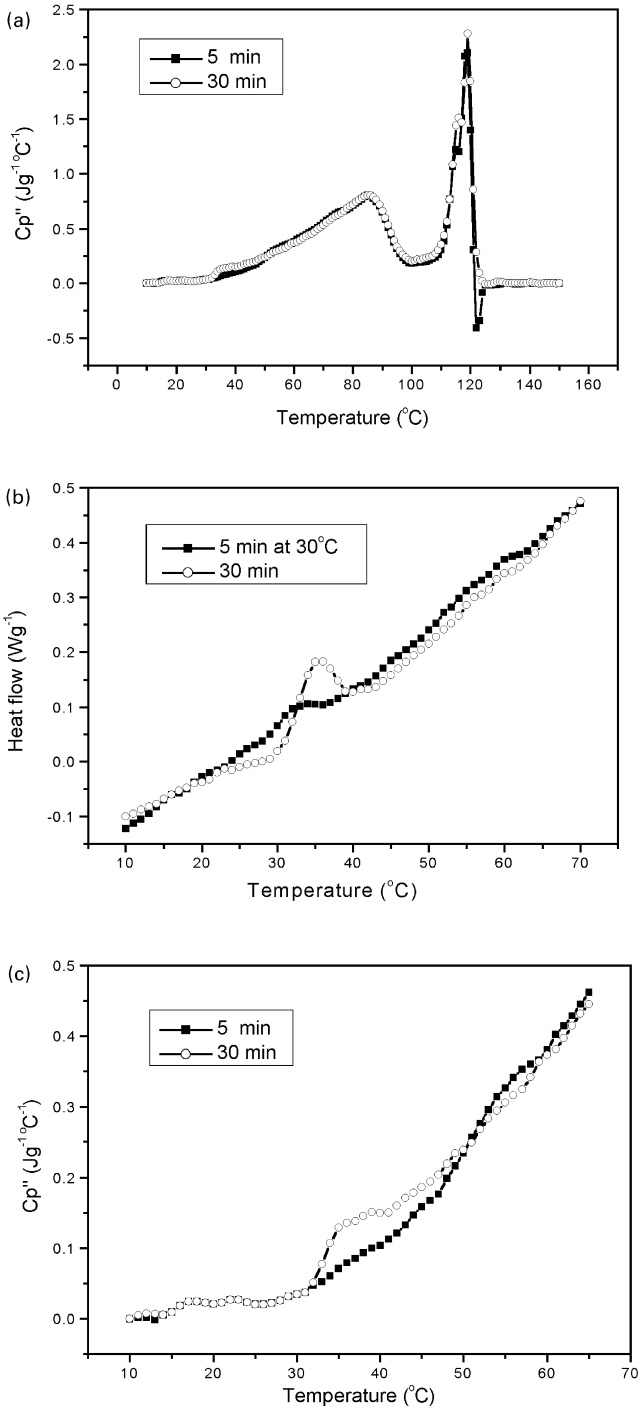

Fig. 7. (a) Plots of imaginary part of complex heat capacity C''_p as a function of temperature, $C''_p = C^*_p \sin \phi$. (b) Local part of Fig. 6a. Note that the data in Fig. 7b has been timed by (−1). (c) Local part of Fig. 7a.

7a, respectively and the data of Fig. 7b has been timed −1. It is obvious to see that both heat flow and C''_p increase with increasing secondary crystallization time. The imaginary part of complex heat capacity obtained from M-TDSC has been demonstrated to correlate with the entropy change of a complete process [21,22]. Thus, the increase of C''_p in magnitude with time indicates that the secondary crystallization process really accompanied with the decreasing conformational entropy of the remaining amorphous. However, heat flow and C''_p change with time in different degree when comparing Fig. 7b and c, which suggests that another process may contribute to the heat flow besides the entropy change.

4. Discussion

As suggested in Section 1, the origin of the crystallization time dependence of the low temperature endotherm temperature can be contributed by several phenomena such as: lamellar thickening, reorganization of amorphous regions, rejection of defects from crystals, crystallization of amorphous chain segments and the steady decrease in the conformational entropy of the remaining amorphous fraction as a result of secondary crystallization recently proposed by Alizadeh et al. [4]. Among them, lamellar thickening and increasing of lateral dimension are almost impossible in the case of ethylene/α-olefin copolymers because of the exclusion of branches and overcrowding effect. In the case of defect diffusion process, it is thermally activated and thus should exhibit higher rates at higher temperatures.

The actual melting point of a polymer crystal was proved to be related to its shape and surface energies through the relationship [26]:

$$T_m = T_m^0\left(1 - \frac{2\sigma_e}{\Delta H^0 \rho_c l} - \frac{4\sigma}{\Delta H^0 \rho_c a} - \frac{c_d \bar{\varepsilon}_d}{\Delta H^0 \rho_c}\right) \quad (2)$$

where σ_e and σ are the surface free energies of the folding and lateral surfaces, respectively, of a prismatic crystal with thickness l and cross section a [2]; c_d is the concentration of all kinds of defects in the crystals and $\bar{\varepsilon}_d$ is the associated mean value of excess free energy. ΔH^0 is the melting enthalpy of the crystal and ρ_c is the density of the crystal phase, T_m^0 is the equilibrium melting point. For polyethylene $T_m^0 = 418.7$ K [27] and $\Delta H^0 = 293$ J/g [8].

From this equation, Alfonso et al. [19] derived the following equation containing the activation energy term.

$$\ln(C/t^*) = \ln(K_0 T/A) - E_t/RT = A - E_t/RT \quad (3)$$

where t^* is the temperature dependent time necessary to obtain crystals with a melting temperature T_m^* in the course of secondary crystallization. A is a parameter slightly dependent on temperature. E_t presents the activation energy of crystal perfection process, such as rejection of defects, reorganization of the lateral surfaces and so on. Values of

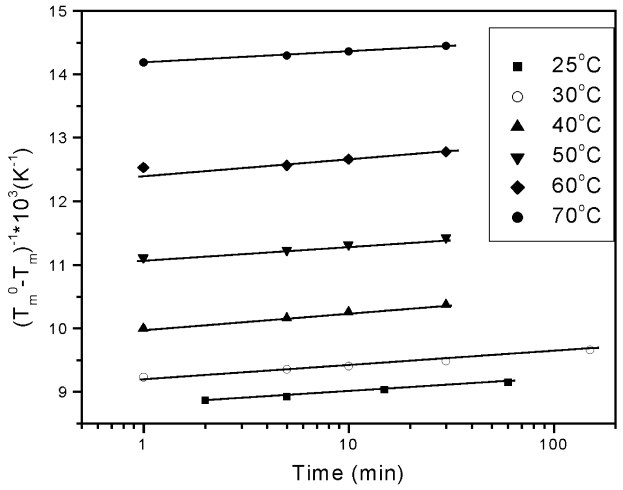

Fig. 8. Relationship between $(T_m^0 - T_m)^{-1}$ and crystallization time and temperature.

C and t^* can be obtained from the plots of $(T_m^0 - T_m^{low})^{-1}$ vs. $\log(t_c)$ (see Fig. 8) and C is the slope of the linearship.

Fig. 9 shows the plots of $\ln(C/t^*)$ vs. $T_c - 1$ for t^* values corresponding to crystals melting at T^* equal to 30, 40, 50 and 60°C. Each set of data can be fitted by two straight lines from which the activation energies reported in Table 2 are obtained. It is surprising to see that the activation energy of low temperature region increases with increasing T^* whereas the activation energy of high temperature region decreases with increasing T^* (see Fig. 10) The crossover will disappear at higher T^*. The calculated activation energies increase with T^* in low temperature region can be accounted for by the crystals perfection process, while the decrease of activation energies in high temperature region indicates that besides the crystals perfection process another process with a negative temperature coefficient must exist at the same time. In the intuitive idea, this process is the steady decrease in conformational entropy of the

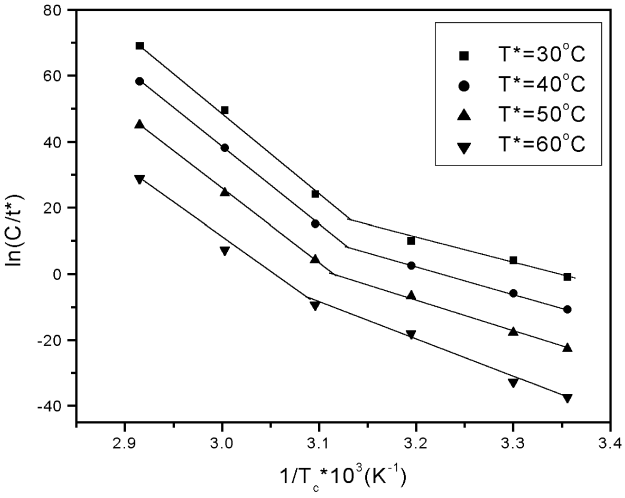

Fig. 9. Plots of experimental values according to Eq. (2).

Table 2
Activation energy (E_t) values from Fig. 9

	T^* (°C)	30	40	50	60
E_t/R	Low temperature region	66.05	81.59	100.4	123.5
	High temperature region	249.5	239.2	226.6	211.8

remaining amorphous fraction as a result of secondary crystallization. As a matter of fact, the crystal perfection and the entropy decrease processes are co-existent during the secondary crystallization. Although these two processes all contribute to the time dependence of the low temperature endotherm, they show different temperature dependence. In low temperature region, the thickness of secondary crystals is very small and the change of conformational entropy is also small. So the apparent activation energy E_t increases with T^*. In high temperature region, the thickness of secondary crystals increases dramatically, and the conformation entropy of amorphous phase decreases dramatically, which decrease the mobility of defects and chain segments and restrain the crystal perfection process, consequently, the apparent activation energy E_t decrease with T^*.

M-TDSC results also suggest the co-existence of these two processes. As shown in Fig. 7b and c, an obvious endothermic peak appears in the plot of heat flow after 5 min secondary crystallization at 30°C, whereas the plot of C''_p changes little. When crystallization time increases to 30 min, both the location and area of low temperature endotherm increase in the plot of heat flow while only a shoulder exists in the plot of C''_p. This result indicates that the decreasing of conformational entropy of residual amorphous is not the sole process during secondary crystallization and the crystal perfection process also exists simultaneously.

5. Conclusions

Based on the standard DSC and M-TDSC experiments on crystallization and melting behavior of short ethylene sequence of metallocene ethylene/α-olefin copolymer with higher comonomer content, we conclude:

1. Time and temperature dependence of low temperature endotherm was shown: T_m^{low} varies linearly with the logarithm of time and the slopes D decrease with increasing secondary crystallization temperature.
2. The location of low temperature endotherm strongly depends on the thermal history before secondary crystallization, and an extrapolation of T_m^{low} (30.6°C) to a few seconds was obtained after two step isothermal crystallization before secondary crystallization at 30°C. The value of T_m^{low} slightly higher than T_c indicates that the initial crystallization at low temperature is nearly reversible.
3. Direct evidence of conformational entropy change of secondary crystallization was obtained by using M-TDSC technique. Both the M-TDSC result and the activation energy analysis of temperature dependence suggest that crystal perfection process and conformational entropy decreasing in residual amorphous co-exist during secondary crystallization.

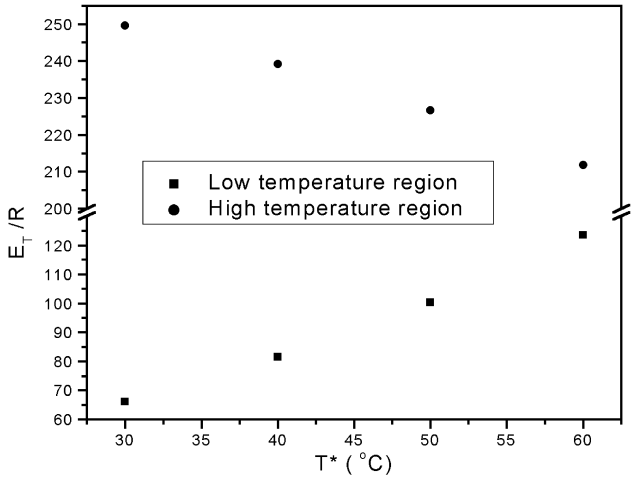

Fig. 10. Plots of activation energy as a function of T^*.

Acknowledgements

This work is subsidized by the Special Funds for Major State Basic Research Projects of China and supported by the National Science Foundation of China. The authors wish to thank Dr Eric T. Hsieh (Phillips Petroleum Company, Bartlesville, Oklahoma, 74004, USA), for kindly supplying samples and useful discussions.

References

[1] Zhang FJ, Liu JP, Xie FC, Fu Q, He TB. Submitted for publication.
[2] Zhang FJ, Liu JP, Fu Q, Huang HY, Hu ZJ, Yao S, Cai XY, He TB. Submitted for publication.
[3] Flory PJ. Trans Faraday Soc 1955;51:848–57.
[4] Alizadeh A, Richardson L, Xu J, McCartney S, Marand H, Cheung YW, Chum S. Macromolecules 1999;32:6221–35.
[5] Androsch R, Wunderlich B. Macromolecules 1999;32:7233–47.
[6] Fu Q, Chiu F, McCreight K, Guo M, Tseng WW, Cheng SZD, Keating MY, Hsieh ET, Deslariers PJ. J Macromol Sci Phys 1997;B36:41–60.
[7] Bensason S, Minick J, Moet A, Chum S, Hiltner A, Baer E. J Polym Sci Part B: Polym Phys 1996;34:1301–15.
[8] Peeters M, Goderis B, Vonk C, Reynaers H, Mathot V. J Polym Sci Part B: Polym Phys 1997;35:2689–713.
[9] Peeters M, Goderis C, Reynaers H, Mathot V. J Polym Sci Part B: Polym Phys 1999;37:83–100.
[10] Crist B, Williams DN. J Macromol Sci Phys 2000;B39:1–13.
[11] Crist B, Howard PR. Macromolecules 1999;32:3057–67.
[12] Crist B, Claudio ES. Macromolecules 1999;32:8945–51.
[13] Minick J, Moet A, Hiltner A, Baer E, Chum SP. J Appl Polym Sci 1995;58:1371–84.
[14] Wang C, Chu MC, Lin TL, Lai SM, Sih HH, Yang JC. Polymer 2001;42:1733–41.

[15] Sehanobish K, Patel RM, Croft BA, Chum SP, Kao C. J Appl Polym Sci 1994;51:887.
[16] Maderek E, Strobl GR. Makromol Chem 1983;184:2553–61.
[17] Alamo R, Mandelkern K. J Polym Sci Part B: Polym Phys 1986;24:2087–105.
[18] Schouterden P, Groenickx G, Van der Heijden B, Jansen F. Polymer 1986;28:2099–104.
[19] Alfonso GC, Pedemonte E, Ponzetti L. Polymer 1979;20:104–12.
[20] Seferis JC, Salin IM, Gill PS, Reading M. Proc Acad Greece 1992;67:311.
[21] Schawe JEK. Thermochim Acta 1997;304/305:111.
[22] Hutchinson JM, Montserrat S. Thermochim Acta 1997;304/305:257.
[23] Song M, Hourston DJ, Pollock HM, Schafer FU, Hammiche A. Thermochim Acta 1997;304/305:335.
[24] Song M. J Therm Anal Calorimet 2001;63:699–707.
[25] Hsieh ET, Tso CC, Byers JD, Johnson TW, Fu Q, Cheng SZD. J Macromol Sci Phys 1997;B36:615–28.
[26] Hoffman JD. SPE Trans 1964;4:315.
[27] Mandelkern L, Alamo RG. In: Mark JE, editor. Physical properties of polymers handbook, Woodbury, NY: American Institute of Physics, 1996. p. 11, chapter 11.